TECHNISCHE MECHANIK
European Journal of Engineering Mechanics
Diamond Open Access

journal homepage: www.ovgu.de/techmech

Tech. Mech., Vol. 46, Is. 1, (2026), 78–92

Received: 29.10.2025
Accepted: 08.01.2026
Available online: 16.02.2026

Enhanced LES-based Turbulent Subcooled Flow Boiling Prediction

Hanan Aburema[1]*, Bruce C. Hanson[1], Michael Fairweather[1], and Marco Colombo[2]

[1] School of Chemical & Process Engineering, University of Leeds, Leeds LS2 9JT, UK
[2] School of Mechanical, Aerospace & Civil Engineering, University of Sheffield, Sheffield S10 2TN, UK

Abstract: High heat transfer rates in many cooling systems are often achieved through subcooled boiling flows along heated walls, where boiling ensures the system's thermal integrity. Understanding boiling mechanisms in turbulent subcooled flows, and improving the accuracy of predictive methods is, in particular, critical for enhancing the design and increasing the safety margins of existing nuclear reactor designs, and accelerating the development and roll out of new designs. This study evaluates two boiling models coupled with large eddy simulations based on a dynamic subgrid-scale model. One boiling model utilises a mechanistic force balance approach to predict bubble dynamics, considering bubble growth and detachment influenced by micro-layer evaporation, superheated liquid heat transfer, and condensation on the bubble cap. The other model employs a reduced correlation-based method to estimate bubble departure diameter and frequency, aiming to maintain reasonable accuracy while reducing computational cost and calibration requirements. Both models are validated against experimental data for vertically upward subcooled boiling flows of water and refrigerant R12 across a wide range of operating conditions. Results show that both approaches achieve satisfactory predictive accuracy and outperform an equivalent Reynolds-averaged Navier-Stokes approach. The mechanistic model provides superior precision in capturing bubble dynamics but at higher computational expense, whereas the correlation-based model offers an efficient alternative suitable for some engineering applications. These findings advance the development of high-fidelity boiling models for nuclear thermal hydraulic simulations and provide a foundation for future research developments and industrial applications.

Keywords: Subcooled boiling, bubble dynamics, large eddy simulation, force balance model, reduced correlation

1 Introduction

Boiling of turbulent subcooled flows is crucial for achieving efficient heat transfer, particularly in thermal hydraulic systems, making it a key focus for researchers in both industry and academia. Subcooled flow boiling plays a critical role in applications requiring effective cooling, such as nuclear reactors, refrigeration systems, and in the chemical process industries Dhir (1998). However, this process is highly complex due to the intricate dynamics of bubble nucleation, growth, detachment, and dispersion near heated surfaces. A comprehensive understanding of these phenomena is crucial for optimising system designs, enhancing performance, and ensuring the reliability and safety of advanced thermal systems.

The transient and complex nature of boiling phenomena makes it difficult to fully understand their underlying physical mechanisms. Experimental studies have primarily aimed at developing empirical correlations based on extensive datasets obtained under diverse geometries, fluid types, and operating conditions Fang et al. (2017); Zhou et al. (2017). However, these experiments are expensive, and the resulting correlations are limited to the specific conditions and setups used. To overcome these limitations, computational fluid dynamics (CFD), and particularly Eulerian–Eulerian approaches, have been widely employed to model flow boiling, providing a more adaptable and cost-effective tool for investigating these processes Colombo and Fairweather (2016). In this approach, the conservation equations for mass, momentum, and energy are solved separately for each phase. However, this method simplifies the system by averaging the phase occurrence over time and space, which results in the loss of detailed interface structure information. As a result, additional models are required to account for the exchange of mass, momentum, and energy between the phases Prosperetti and Tryggvason (2009). The phase change at the heated wall and the distribution of heat flux between the liquid and vapour phases are typically modelled using wall boiling models. One of the most widely used heat flux models is the Rensselaer Polytechnic Institute (RPI) model Kurul and Podowski (1990), in which the external heat flux applied to the heating wall is partitioned into three primary heat transfer mechanisms: single-phase convection, quenching, and evaporation. These mechanisms depend on several key parameters, including nucleation site density, bubble departure diameter, and bubble departure frequency, with correlations for these quantities initially derived from pool boiling experiments conducted at ambient pressure Tolubinsky and Kostanchuk (1970). A detailed review of the available correlations can be found in Yeoh et al. (2014). Numerous studies have evaluated the applicability of the RPI model using the standard correlations implemented in most CFD packages. However, these studies have shown that the model often exhibits limited accuracy and generality Colombo and Fairweather (2016).

Among the key parameters requiring accurate modelling, the bubble departure diameter is particularly important for predicting the void fraction distribution within the flow. Consequently, mechanistic sub-models that explicitly describe bubble dynamics are essential for improving predictive accuracy. Klausner et al. (1993) developed a mechanistic model based on a force balance during the bubble's growth phase prior to its departure from a surface. This model demonstrated good predictive performance against their experimental data. Over the years, many researchers have worked on improving the original model to increase its

---

* E-mail address: h.aburema@leeds.ac.uk

doi: 10.24352/UB.OVGU-2026-009

predictive capability across a wider range of experimental conditions Sugrue and Buongiorno (2016). One significant enhancement involved incorporating local condensation effects into the bubble growth rate model, along with modifications to the lift force and surface tension models Yun et al. (2012). Further improvements were made by integrating microlayer evaporation beneath the bubble to enhance model accuracy Colombo and Fairweather (2015b). Recent research conducted at the Massachusetts Institute of Technology (MIT) has introduced a comprehensive approach to heat flux partitioning by incorporating all essential wall nucleation closures Kommajosyula (2020). Using experimental data obtained through advanced measurement techniques, the MIT model provides wall nucleation closures that are applicable across a wide range of pressures and flow conditions. Unlike conventional models, this approach eliminates the need for case-specific calibration, improving its adaptability and reliability Pham et al. (2023). Most existing modelling efforts for subcooled boiling have also relied on Reynolds-averaged Navier–Stokes (RANS) approaches due to their relatively low computational cost. However, RANS models tend to over-predict mixing and fail to capture the complex transient dynamics of turbulent flow boiling due to their inherent averaging of turbulent fluctuationsColombo and Fairweather (2015a, 2016); Colombo et al. (2019). To address these limitations, researchers have increasingly turned to large eddy simulation (LES), which offers a more accurate and robust framework for studying complex flows and boiling phenomena Owoeye and Schubring (2016). Although LES requires significantly greater computational resources than RANS-based approaches, continuous advancements in computing power are making it increasingly feasible for high-fidelity analysis and optimisation of boiling flows. In this study, the bubble dynamics model and the reduced-correlation MIT model are implemented in the OpenFOAM code and compared within an LES framework. LES allows a detailed investigation of subcooled boiling flows, offering improved accuracy in capturing key phenomena. Both models are validated against experimental data for vertically upward boiling flows of water and refrigerant R12 (Freon-12, dichlorodifluoromethane) over a wide range of conditions.

2 Numerical Model

The Eulerian–Eulerian two-phase flow model describes each phase (e.g., liquid (L) and gas (G)) by a set of averaged continuity, momentum, and energy conservation equations. These equations are weighted by the local volume fraction, indicating the portion of the total volume occupied by each phase, and vary continuously in space and time:

$$\frac{\partial(\alpha_L\rho_L)}{\partial t} + \nabla\cdot(\alpha_L\rho_L\mathbf{u}_L) = \Gamma_{LG} - \Gamma_{GL} \tag{1}$$

$$\frac{\partial(\alpha_L\rho_L\mathbf{u}_L)}{\partial t} + \nabla\cdot(\alpha_L\rho_L\mathbf{u}_L\mathbf{u}_L) = -\alpha_L\nabla p + \alpha_L\rho_L\mathbf{g} - \nabla\cdot(\alpha_L\tau_L) + M_I \tag{2}$$

$$\frac{\partial(\alpha_L\rho_L(H_L+K_L))}{\partial t} + \nabla\cdot(\alpha_L\rho_L\mathbf{u}_L(H_L+K_L)) = \nabla\cdot(\alpha_L D_{eff}\nabla H_L) + \alpha_L\frac{\partial p}{\partial t} + \alpha_L\mathbf{g}\cdot\mathbf{u}_L + \Gamma_{GL}K_G - \Gamma_{GL}K_L + Q_L \tag{3}$$

Here, Γ_{GL} is the mass transfer from phase G to phase L and Γ_{LG} is the mass transfer from phase L to phase G, with Q_L the energy transfer due to sensible heat transfer and phase change across the interface.

2.1 Interfacial Momentum Transfer Forces

Due to the averaging procedure in the Eulerian–Eulerian model, details of the interfacial structure are not explicitly resolved, and closure models are required to represent the transfer of mass, momentum, and energy between phases. The interfacial momentum transfer term M_I in Eq. 2 models the dynamic interaction between the phases, and incorporates contributions from several forces.These include drag, lift, wall lubrication, turbulent dispersion, virtual mass, surface tension, and phase change mass transfer forces, particularly in the context of boiling flow:

$$M_I = F_d + F_l + F_{wl} + F_{td} + F_{vm} + F_{st} + F_{mt} \tag{4}$$

The drag force is the resistance experienced by a bubble as it moves through the liquid, modelled as:

$$F_d = \frac{3}{4}\frac{C_d}{d_B}\alpha_G\rho_L(\mathbf{u}_G - \mathbf{u}_L)|\mathbf{u}_G - \mathbf{u}_L| \tag{5}$$

The drag coefficient C_d is calculated using the drag model proposed by Tomiyama et al. (1998), as it incorporates the influence of bubble deformation and provides a smooth transition between spherical and deformed bubbles:

$$C_d = \max\left(\frac{24}{Re_B}(1+0.1\mathrm{Re}_B^{0.75}), \frac{8}{3(\mathrm{Eo}+4)}\right) \tag{6}$$

Here, Re_B is the bubble Reynolds number(= $u_r d_B/\nu$) and Eo the Eötvös number (= $\Delta\rho g d_B^2/\sigma$). Bubbles moving in a shear flow experience a lift force perpendicular to their direction of motion, influencing the radial void distribution in pipes, with small bubbles pushed towards the wall, while larger bubbles tend to move toward the pipe centre after reaching a critical diameter. The wall force, on the other hand, keeps bubbles away from the wall. However, due to the limited understanding of the contributions of lift and wall forces in boiling flows Colombo and Fairweather (2016), these forces are neglected in this study. The turbulent dispersion force is a modelling term introduced in Euler–Euler formulations to represent the redistribution of the dispersed phase caused by turbulent fluctuations. This closure influences the sharpness of the wall peak of the void fraction profile. In the present study, the de Bertodano (1998) model is used with a turbulent dispersion coefficient $C_{td} = 0.7$ to balance the dispersion of vapour bubbles where increased turbulence due to phase change requires a stronger dispersion effect Kurul and Podowski (1990); Leonar (1975).

$$F_{td} = k\nabla\alpha_G\rho_L C_{td} \tag{7}$$

The virtual mass force is the inertia added to the system because an accelerating or decelerating bubble must move the surrounding fluid as it moves through it Jakobsen et al. (1997), which is modelled as:

$$F_{vm} = \alpha_G\rho_L C_{vm}\left(\frac{D\mathbf{u}_G}{Dt} - \frac{D\mathbf{u}_L}{Dt}\right) \tag{8}$$

A fixed coefficient of $C_{vm} = 0.5.$ is employed. The phase change mass transfer force accounts for the momentum transferred between phases due to phase change processes (i.e. evaporation or condensation) in boiling flows.This force ensures conservation of momentum in the system by incorporating the momentum entering and leaving the phase during mass transfer Greenshields (2019), which can be stated as:

$$F_{mt} = \Gamma_{GL}\mathbf{u}_G - \Gamma_{LG}\mathbf{u}_L \tag{9}$$

2.2 Population Balance Model

The interfacial transport mechanisms in boiling are influenced by the bubble size distribution. To predict the bubble size distribution and the bubble average diameter, the Multiple Size Group (MUSIG) population balance approach is used, which is part of the OpenFOAM code Greenshields (2019). In this model, the bubble diameter distribution is discretised into a finite number of classes. Each class is characterised by a diameter and a gas volume fraction, with the total gas volume fraction given by:

$$\alpha_G = \sum_{i=1}^{M}\alpha_i \tag{10}$$

The relative volume density of each class is defined as:

$$f_{G,i} = \frac{\alpha_i}{\alpha_G}, \quad \sum_{i=1}^{M} f_{G,i} = 1 \tag{11}$$

The transport equation for each bubble size group accounts for advection and sources resulting from bubble interactions and phase change:

$$\frac{\partial}{\partial t}(\alpha_i\rho_G f_{G,i}) + \nabla\cdot(\alpha_i\rho_G\mathbf{u}_G f_{G,i}) = S_i^{topo} + S_i^{phase} \tag{12}$$

Here, S_i^{topo} (i.e. the birth and death of bubbles due to coalescence and breakup) with bubble coalescence modelled according to Prince and Blanch (1990) and break-up based on Lehr et al. (2002). The term S_i^{phase} represents condensation and evaporation effects. The Sauter mean diameter is calculated as:

$$d_{B,SMD} = (\sum_{i=1}^{M}\frac{f_{G,i}}{d_{G,i}})^{-1} \tag{13}$$

In this study, 14 bubble classes were used to balance accuracy with computational cost Krepper et al. (2008), covering bubble diameters in the range of 0.1–1.4 mm, consistent with bubble sizes observed in the experiments used for model validation.

2.3 Large Eddy Simulation

The LES equations are obtained by spatially filtering the governing transport equations, Eqs. 1–3, such that large-scale turbulent motions are explicitly resolved, while small subgrid-scale (SGS) fluctuations must be modelled to close the system. The influence of the unresolved scales on the resolved scales is represented through the SGS stress tensor, which is modelled as:

$$\tau_L^{sgs} = -\mu_L^{eff} \left(\nabla \mathbf{u}_L + (\nabla \mathbf{u}_L)^T - \tfrac{2}{3} I (\nabla \cdot \mathbf{u}_L) \right) \tag{14}$$

For the liquid phase, the effective viscosity $\mu^{eff,L}$ is determined by considering the molecular viscosity, turbulent viscosity and bubble-induced turbulence, with the latter being modelled using approach described by Sato et al. (1981), ensuring an accurate representation of the flow dynamics:

$$\mu_{eff,L} = \mu_L + \mu_{T,L} + \mu_{BI,L} \tag{15}$$

$$\mu_{BI,L} = \rho_L C_{BI} \alpha_G d_B |\mathbf{u}_G - \mathbf{u}_L| \tag{16}$$

In this study, the dynamic Smagorinsky SGS model is used to model the unresolved turbulent viscosity, which relies on applying a second filter considering both spatial and temporal variations:

$$\mu_{T,L} = \rho_L (C_s \Delta)^2 |\bar{S}_{ij}| \tag{17}$$

The precision of the model is improved by accounting for such variations, making it more dependable for capturing flow dynamics. It employs a dynamic procedure to calculate C_s based on the Leonard stress tensor L_{ij} and the Germano rate of strain tensor M_{ij} through an iterative process Germano et al. (1991), with:

$$C_s = \frac{1}{2} \frac{L_{ij} M_{ij}}{M_{ij} M_{ij}} \tag{18}$$

$$L_{ij} = \widehat{\bar{u}_i \, \bar{u}_j} \; - \; \hat{\bar{u}}_i \, \hat{\bar{u}}_j \tag{19}$$

$$M_{ij} = \Delta^2 \, \widehat{\left(\bar{S}_{ij} \, \bar{S}_{ij} \right)} - \hat{\bar{S}}_{ij} \, \hat{\bar{S}}_{ij} \tag{20}$$

The turbulence kinetic energy is modelled based on the dynamic procedure as:

$$k = C_s \Delta^2 S^2 \tag{21}$$

For the gas phase, turbulence is not resolved, and the effects of liquid-phase turbulence on the gas phase are neglected due to the negligible density of air compared to that of the liquid phase. This simplification reduces model complexity and avoids the need for additional equations to account for gas-phase turbulence.

2.4 Wall Treatment

In LES, the accurate representation of the near-wall region is essential due to the significant velocity gradients near a surface. The standard logarithmic law often fails to capture the complexities of non-equilibrium wall functions and pressure gradient effects, especially in the presence of strong turbulence. To overcome these limitations, Spalding's formula Spalding (1961) is used, where the turbulence length scale, y^+, is defined as follows:

$$y^+ = u^+ \frac{1}{E} \left[e^{cu^+} - 1 - cu^+ - \frac{(cu^+)^2}{2} - \frac{(cu^+)^3}{6} \right] \tag{22}$$

where $E = 9.025$ and $c = 0.4$, and the dimensionless parameters y^+ and u^+ are defined as:

$$y^+ = \frac{y u_\tau}{\nu}, u^+ = \frac{u}{u_\tau} \tag{23}$$

Since Spalding's equation is nonlinear, an iterative procedure, such as the Newton-Raphson method, must be used to solve for u_τ.This method ensures rapid convergence and improves the accuracy of near-wall turbulence modelling by capturing velocity variations more effectively, while avoiding the need for excessive mesh refinement. In this study, the first-cell height corresponds to y^+ values in the range of $5 - 20$, consistent with the valid range for Spalding's approach Spalding (1961).

3 Enhanced Wall Boiling Model

In the RPI model, the heat flux imposed on the heated wall is partitioned into three primary contributions: single-phase convection, representing heat transferred directly to the liquid where no bubbles are present; quenching, which accounts for transient heat transfer when cooler liquid rewets the wall after bubble departure; and evaporation, corresponding to the latent heat absorbed during bubble growth and detachment. Hence:

$$q''_{RPI} = q''_c + q''_q + q''_e \tag{24}$$

The single-phase convective heat flux contribution is calculated as:

$$q''_c = h_c(1 - A_B)(T_w - T_L) \tag{25}$$

The boiling fraction area A_B is the portion of the wall surface covered by active nucleating bubbles. The single-phase heat transfer coefficient h_c is modelled as:

$$h_c = \frac{\rho_L c_{p,L} u_{\tau,L}}{T_L^+} \tag{26}$$

Here, T_L^+ is a dimensionless temperature, which is calculated using the wall function approach Greenshields (2019), which accounts for near-wall thermal gradients in turbulent boundary layers. The quenching heat flux is expressed as:

$$q''_q = h_q A_B(T_w - T_L) \tag{27}$$

with the quenching heat transfer coefficient modelled as:

$$h_q = 2 f_{dep} \sqrt{\frac{t_w k_c \rho_L c_{p,L}}{\pi}} \tag{28}$$

The waiting time t_w refers to the interval between the departure of one bubble and the initiation of the next bubble at the same nucleation site and is calculated as:

$$t_w = \frac{0.8}{f_{dep}} \tag{29}$$

The rate of evaporative heat transfer depends on the number of active nucleation sites, the size of the bubbles at the point of departure, the frequency of bubble release, and the latent heat of vaporisation:

$$q''_e = (\frac{\pi d_{dep}^3}{6}) N_a f_{dep} \rho_G h_{LG} \tag{30}$$

Among these terms, the evaporative heat flux is fundamental to nucleate boiling and has a significant impact on the overall thermal behaviour of the heated surface. It is particularly sensitive to the dynamics of bubble nucleation and departure, as it directly represents the energy required for phase change from liquid to vapour at the wall. Accurate modelling of this term is essential for predicting heat transfer performance in boiling systems.

3.1 Bubble Departure Diameter

In the mechanistic approach, the bubble departure diameter is determined by evaluating the balance of forces acting on a single bubble at its nucleation site. During the growth process, the forces acting on the bubble can be classified into x-direction adhesive forces, which keep the bubble attached to the nucleation site, and y-direction detaching forces which act to separate the bubble from the surface. When the resultant detaching forces exceed the adhesive forces, the bubble departs from the nucleation site. Similarly, for a sliding bubble, if the detaching forces surpass the adhesive forces, the bubble lifts off from the heated surface and moves toward the bulk flow. The various forces influencing bubble growth at the nucleation site are shown schematically in Fig. 1. The force balance equations are expressed as:

$$\sum F_x = F_{st,x} + F_{qsd} + F_b \sin\theta + F_{ud,x} \tag{31}$$

$$\sum F_y = F_{st,y} + F_{sl} + F_b \cos\theta + F_{ud,y} + F_p + F_{cp} \tag{32}$$

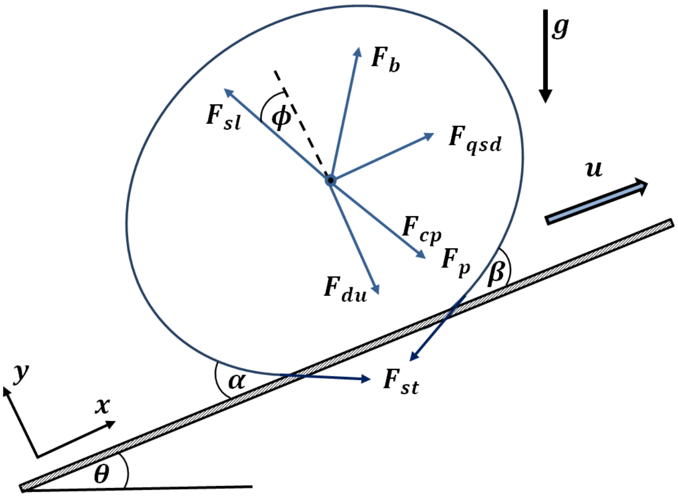

Fig. 1: Forces acting on a bubble at the nucleation site

In Eq. 31 and Eq. 32, F_{st} is the surface tension force, F_{qsd} the quasisteady drag force, F_b the buoyancy force, F_{ud} the unsteady drag force caused by asymmetrical bubble growth, F_{sl} the shear lift force, F_p the hydrodynamic pressure force, and F_{cp} the contact pressure force, with subscripts x and y referring to forces acting in the x and y directions. An analytical formula for the surface tension forces acting on a growing bubble at the heated wall is obtained by integrating the surface force along the contact line between the bubble and the heated wall Klausner et al. (1993):

$$F_{st,x} = -1.25 d_w \sigma \frac{\pi(\alpha-\beta)}{\pi^2-(\alpha-\beta)^2}(\sin\alpha + \sin\beta) \tag{33}$$

$$F_{st,y} = -d_w \sigma \frac{\pi}{(\alpha-\beta)}(\cos\beta - \cos\alpha) \tag{34}$$

The advancing (α) and receding (β) contact angles are used to characterise the bubble's interaction with the heated surface.$\alpha = \pi/4$ and $\beta = \pi/5$ are adopted, as recommended in Klausner et al. (1993). The bubble wall contact diameter (d_w) is estimated as a fraction of the bubble departure diameter, with a commonly adopted value of $d_w = d_{dep}/15$, as recommended in Yun et al. (2012). The quasi-steady drag force acting on a spherical bubble in a uniform, unbounded liquid flow was formulated by Mei and Klausner (1992) to account for the effects of Reynolds number and bubble motion. It is expressed as:

$$F_{qsd} = 6\pi\rho_L \nu u R^{2/3}(\tfrac{2}{3} + [(\tfrac{12}{\mathrm{Re}})^{0.65} + 0.862]^{-1.54}) \tag{35}$$

The shear lift force is included in the bubble departure model because it directly influences bubble detachment from the heated wall by contributing to the net upward forces on the bubble Klausner et al. (1993). It is formulated as an interpolation between two models: one applicable to spherical bubbles in viscous flows at low Reynolds numbers Mei and Klausner (1992), and the other suited for inviscid flows with low shear rates Auton (1987). This hybrid formulation enhances the model's applicability across a broader range of flow conditions, improving the accuracy of shear lift force predictions, and is given by:

$$F_{sl} = \tfrac{1}{2}\pi\rho_L u R^2 (3.877 G_s^{0.5}[\mathrm{Re}^{-2} + (C_l G_s^{0.5})^4]^{1/4}) \tag{36}$$

In this equation the dimensionless shear rate of the incoming flow is calculated as follows:

$$G_s = |\tfrac{du}{dy}|\tfrac{R}{u} \tag{37}$$

The unsteady drag force due to asymmetric growth of the bubble is expressed as a transient force component that accounts for the added mass effect caused by the accelerating fluid around the expanding bubble:

$$F_{ud,x} = -\rho_L \pi R^2 \left(\tfrac{2}{3}\dot{R}^2 + R\ddot{R}^2\right)\sin\varphi \tag{38}$$

$$F_{ud,y} = -\rho_L \pi R^2 \left(\tfrac{2}{3}\dot{R}^2 + R\ddot{R}^2\right)\cos\varphi \tag{39}$$

The inclination angle (φ), defined in the y-direction, is set to $\varphi = \phi/18$ as adopted in Klausner et al. (1993). The buoyancy force on a bubble, due to the difference in density between the liquid and vapour phases, is determined using the density variation and the bubble size:

$$F_b = \tfrac{4}{3}\pi R^3(\rho_L - \rho_G)g \tag{40}$$

The last terms in the y-direction force balance correspond to the hydrodynamic pressure and contact pressure forces, and are expressed as:

$$F_p = \tfrac{9}{8}\rho_L u^2 \pi \frac{d_w^2}{4} \tag{41}$$

$$F_{cp} = \sigma R \pi \frac{d_w^2}{4} \tag{42}$$

To accurately capture the dynamics of bubble detachment and heat transfer during nucleate boiling, accurate modelling of the bubble growth process is essential. Before detachment, the bubble diameter evolves according to a defined growth equation. Recently, Colombo and Fairweather (2015b)proposed a combined equation that integrates the contributions of superheating and subcooling in predicting the bubble growth rate during flow boiling, with Fig. 2 illustrating these mechanisms. In their approach, evaporation from the thin liquid micro-layer beneath the growing bubble is considered a key heat transfer mechanism. The evaporation rate is evaluated using the correlation proposed by Cooper and Lloyd (1969):

$$\frac{dR(t)}{dt} = \frac{1}{C_2}\mathrm{Pr}^{-0.5}\mathrm{Ja}_{sup}\left(\frac{k_c}{\rho_L c_{p,L}}\right)^{0.5} t^{-0.5} \tag{43}$$

The constant C_2 denotes the initial thickness of the micro-layer, with an optimised value of 1.78 used in this study. The heat transfer from the adjacent superheated boundary layer, based on Plesset and Zwick (1954) is given by:

$$\frac{dR(t)}{dt} = \sqrt{\frac{3}{\pi}}(T_{L,sup} - T_{sat})\left(\frac{\lambda_L}{\rho_L c_{p,L}}\right)^{0.5}(1-b)t^{-0.5} \tag{44}$$

The model also considers condensation occurring at the bubble cap when it interacts with the surrounding subcooled liquid, with the condensation heat transfer coefficient estimated using the Ranz and Marshall (1952) correlation:

$$\frac{dR(t)}{dt} = -\frac{h_c}{\rho_L h_{lg}}(T_{sat} - T_{sub})b \tag{45}$$

Here the parameter (b) indicates the area of the bubble surface that interacts with the subcooled liquid. It is evaluated by locating the point in the thermal boundary layer where the fluid temperature within that layer reaches saturation, using a temperature distribution scaled according to the single-phase wall function developed by Kader (1981).

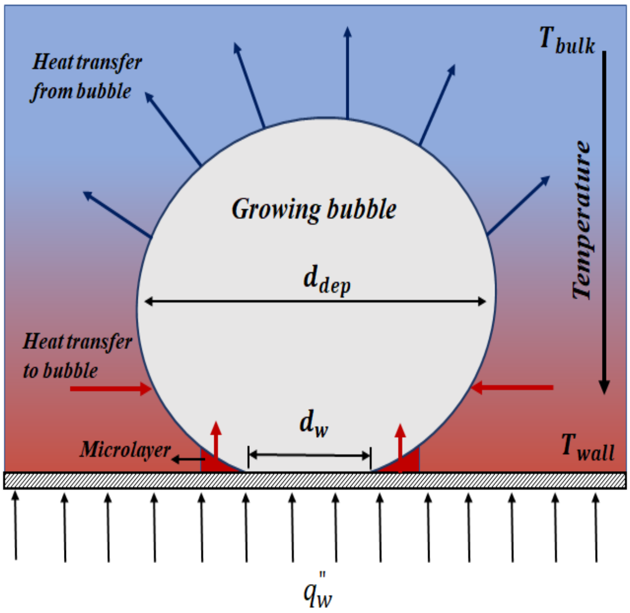

Fig. 2: Schematic representation of the heat transfer mechanisms during bubble growth

By incorporating the combined effects of micro-layer evaporation, thermal diffusion from the superheated boundary layer and condensation at the bubble cap due to the subcooled liquid, the total bubble growth equation is expressed as:

$$\frac{dR(t)}{dt} = \frac{1}{C_2}\mathrm{Pr}^{-0.5}\mathrm{Ja}_{sup}\left(\frac{k_c}{\rho_L c_{p,L}}\right)^{0.5} t^{-0.5} + \frac{3}{\pi}(T_{L,sup} - T_{sat})\left(\frac{\lambda_L}{\rho_L c_{p,L}}\right)^{0.5}(1-b)t^{-0.5} - \frac{h_c}{\rho_L h_{lg}}(T_{sat} - T_{sub})b \tag{46}$$

In the MIT framework Kommajosyula (2020), the departure diameter refers to the bubble size at the moment it detaches from the nucleation site, either by sliding along the heated surface or by moving into the bulk liquid. In contrast, the lift-off diameter describes the size of a sliding bubble at the instant it detaches from the heated surface entirely and moves into the bulk flow. The departure diameter is expressed as follows:

$$d_{dep} = 18.6 \times 10^{-}6\left(\frac{\nabla\rho}{\rho_G}\right)^{0.27}(\mathrm{Ja}_{sup})^{0.75}(1+\mathrm{Ja}_{sub})^{-0.3}(u_L)^{-0.26} \tag{47}$$

Although this model does not explicitly resolve individual detachment forces, it provides a robust and computationally efficient method for estimating the bubble departure diameter across a wide range of operating conditions. In this study, the detached bubble diameter is determined differently depending on the model. In the force-balance (FB) framework, the departure diameter is obtained by integrating the bubble growth equation while evaluating the balance of forces at the wall, allowing the bubble to expand until detaching forces overcome adhesive forces. In contrast, the MIT model estimates the departure diameter using the correlation proposed by Kommajosyula (2020), which does not explicitly resolve individual detachment forces. Consequently, differences in predicted departure diameters between the FB and MIT models can occur, particularly under conditions where force interactions at the wall significantly influence bubble growth and detachment. Once detached, the average bubble diameter across the pipe is computed by the population balance model, which accounts for bubble size distributions influenced by coalescence and breakup.

3.2 Bubble Departure Frequency

Bubble departure frequency is a key factor in boiling heat transfer, describing how often a bubble forms, grows, and detaches from a single nucleation site. One of the earliest and still widely used methods is a correlation introduced by Cole (1960). This method estimates the departure frequency using the size of the departing bubble and its rising speed in the liquid:

$$f_{dep} = \sqrt{\frac{3}{4}\frac{g(\rho_L - \rho_G)}{d_w \rho_L}} \tag{48}$$

Another essential parameter in the MIT framework Kommajosyula (2020) is the bubble departure frequency, which is determined by incorporating the bubble wait time and an improved representation of bubble growth dynamics, derived from a force balance approach, with:

$$f_{dep} = \frac{1}{t_{growth} + t_{wait}} \tag{49}$$

The bubble growth time rate is represented by a bubble growth constant K, which accounts for thermal and fluid properties:

$$t_{growth} = \left(\frac{d_{dep}}{4K}\right)^2 \tag{50}$$

$$K = \frac{\sqrt{\lambda_L}}{0.804\sqrt{\mathrm{Pr}}}\mathrm{Ja}_{sup} + \chi 1.95\mathrm{Ja}_{sup}\lambda_L \tag{51}$$

To account for the effects of saturated and subcooled boiling regimes, a parametric coefficient (χ) is introduced, which reflects the level of subcooling ($\chi = A - B\zeta$) where $\zeta = \Delta T_{sub}/\Delta T_{sup}$. For saturated conditions ($\zeta = 0$), the coefficient $A = 1.55$ was obtained through fitting of data from Klausner et al. (1993). The waiting time duration is influenced by flow subcooling and wall superheat and is estimated using a semi-empirical correlation developed through curve fitting of experimental data from multiple sources:

3.3 Nucleation Site Density

Lemmert and Chawla (1977) proposed a correlation for estimating the density of active nucleation sites as a function of wall superheat, recognising that the number of sites increases with the level of surface overheating:

$$N_a = C_n N_{ref}\left(\frac{T_w - T_L}{\Delta T_{ref}}\right)^n \tag{52}$$

with an empirical constant $C_n = 1.0$, and the reference number of nucleation bubbles per unit area taken as $N_{ref} = 3 \times 10^7\,\mathrm{m}^{-2}$. The reference superheat temperature $\Delta T_{ref} = 10\,K$, and $n = 1.805$. A more advanced model proposed by Hibiki and Ishii (2003) accounts for the contact angle to improve the accuracy and generality of nucleation site density predictions:

$$N_a = N_{ref}\left[1 - \exp\left(-\frac{\theta^2}{8\mu'^2}\right)\right]\left[\exp\left(f_0\frac{\lambda_c}{R_c}\right) - 1\right] \tag{53}$$

with $N_{ref} = 4.72 \times 10^5\,\mathrm{m}^{-2}$, $\mu' = 0.755\,\mathrm{rad}$ and $\lambda_c = 2.5 \times 10^{-6}\,\mathrm{m}$. R_c is the critical bubble radius and f_0 is a function of the fluid properties, calculated as:

$$R_c = \frac{2\sigma\left[1 + \sigma_G/\sigma_L\right]/p}{\exp\left[h_{lg}\left(T_G - T_{sat}\right)/\left(R_g T_G T_{sat}\right)\right] - 1} \tag{54}$$

$$f_0 = -0.01064 + 0.4846\rho^+ - 0.22712\rho^{+2} + 0.05468\rho^{+3} \tag{55}$$

$$\rho^+ = \log\left(\frac{\rho_L - \rho_G}{\rho_G}\right) \tag{56}$$

In this study the force balance and MIT correlations are compared, The closures used with the force balance and MIT frameworks are summarised in Tab. 1.

Tab. 1: Summary of the closures used with the force balance and MIT models.

Model	FB	MIT
Bubble departure diameter	Klausner et al. (1993)	Kommajosyula (2020)
Bubble growth	Colombo & Fairweather (2015)	Kommajosyula (2020)
Bubble departure frequency	Cole (1960)	Kommajosyula (2020)
Nucleation site density	Hibiki & Ishii (2003)	Lemmert & Chawla (1972)

4 Experimental and Numerical Setup

Two experiments were selected to validate the numerical simulations in this study: the DEBORA experiments Garnier et al. (2001), and the experiment of Bartolomei and Chanturiya (1967). The DEBORA experiments investigated subcooled boiling of Freon-12 in a vertical pipe with an inner diameter of 19.2 mm and a length of 3.5 m, simulating high-pressure water boiling at pressures ranging from 1.46 to 3.01 MPa. In contrast, the Bartolomei and Chanturiya (1967) experiment examined subcooled boiling of water in a vertical pipe with a 15.4 mm inner diameter and a heated length of 2 m, operating at pressures up to 15 MPa. These experiments provided critical data, including area-averaged void fractions, wall temperatures, average bubble diameters, and liquid temperatures. These datasets serve as reliable benchmarks for assessing computational fluid dynamic models as they effectively capture boiling conditions relevant to nuclear reactor systems while remaining experimentally accessible. A summary of the experimental conditions studied is given in Tab. 2, and a summary of the liquid and gas properties used in the simulations is given in Tab. 3.

Tab. 2: Summary of the experimental conditions studied.

Experiment	P [MPa]	G [kg/m^{2}s]	q'' [kW/m^2]	T_{in} [K]	T_{sat} [K]	Fluid
DEBORA_1	2.62	1996	73.89	341.67	359.98	R12
DEBORA_2	2.62	1985	73.89	343.68	359.98	R12
DEBORA_3	1.46	2028	76.20	301.67	331.25	R12
DEBORA_4	1.46	2030	76.24	304.31	331.25	R12
Bartolomei and Chanturiya	4.5	900	570.0	470.55	530.55	water

Tab. 3: Liquid and gas properties used in the simulations.

P [MPa]	T_{sat} [K]	ρ_L [kg/m^3]	Cp_L [J/kg·K]	μ_L [kg/m·s]	ρ_G [kg/m^3]	Cp_G [J/kg·K]	μ_G [kg/m·s]	σ [N/m]
2.62	359.98	1016.4	1357.5	8.94×10^{-5}	172.51	1200.7	1.639×10^{-5}	0.00176
1.46	331.25	1177.0	1111.6	1.315×10^{-4}	84.97	861.94	1.341×10^{-5}	0.00465
4.5	530.55	870.6	4461.6	1.373×10^{-4}	22.7	4227.9	1.78×10^{-5}	0.072

The numerical simulations were conducted using a three-dimensional axisymmetric geometry, with the computational domain designed to replicate the experimental setups. To reduce computational cost while maintaining accuracy, a 10° wedge of each pipe was employed as the computational domain. A fully developed velocity profile was specified at the inlet of the domain to ensure representative flow conditions, which is essential for capturing realistic flow behaviour. At the top outlet, a pressure boundary condition was imposed. The heated wall was subjected to a uniform heat flux, with no-slip conditions for the liquid and free-slip for the vapour phase to account for the negligible shear stress at the wall for this phase. The computational mesh consisted of approximately 1.5 Million hexahedral cells, with the axial grid spacing Δx ranged from 3×10^{-4} m at the centreline to 5×10^{-5} m near the wall and within the boiling region, with vertical refinements $\Delta y = 3 \times 10^{-3}$ m and circumferential spacing $\Delta z = 3 \times 10^{-4}$ m. Based on the resolved velocity fluctuations in the LES, approximately 80–90% of the turbulent kinetic energy is resolved in the boiling region, where turbulence intensity is highest. Fig. 3 shows the schematic of the test section with the three-dimensional computational domain and mesh. A central differencing scheme was used for the advection term to minimise numerical diffusion and enhance accuracy. For time discretisation, a second-order backward Euler scheme was selected to improve temporal accuracy and stability. These schemes were chosen to ensure a robust and accurate representation of the complex boiling phenomena under investigation. However, it is important to note that the computational cost varied between the models, with the simulation time using the mechanistic model being approximately twice that of the MIT model, primarily due to the detailed treatment of bubble dynamics, which requires additional computational resources to resolve the small-scale boiling mechanisms accurately.

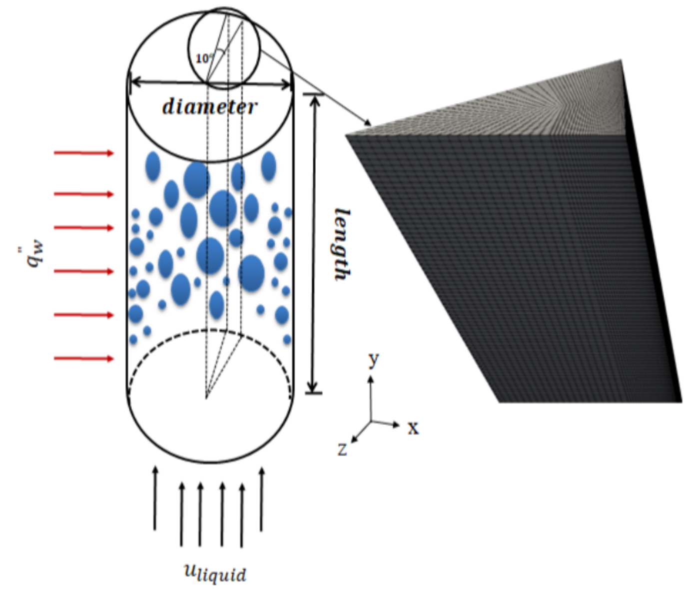

Fig. 3: Schematic view of the test section and the three-dimensional computational domain and mesh

5 Results and Discussion

The results demonstrate the performance of the LES-based framework when coupled with two distinct boiling models: a mechanistic force balance approach and the reduced, correlation-based MIT model. These models are validated using experimental data for vertically upward subcooled boiling flows. In addition, comparisons are made with the study by Colombo et al. (2019) that employed a force balance approach, neglecting subcooling effects, obtained using a RANS-based method closed using a high-Reynolds number multiphase version of the k–ε turbulence model. These RANS simulations were performed only for two cases: DEBORA-2 Garnier et al. (2001) and the Bartolomei and Chanturiya (1967) experiment. The analysis focuses on key parameters, including void fraction distribution, mean bubble diameter, and wall temperature profiles.

5.1 Void Fraction Distribution

The predicted radial void fraction distributions, shown in Fig. 4(a–d) for the DEBORA Garnier et al. (2001) experiments, reveal a wall-peaked distribution, consistent with experimental observations. Both the force balance and MIT models reproduce the characteristic decrease in void fraction from the heated wall toward the bulk flow. The force balance model provides closer agreement with the experimental data, though it slightly over-predicts the void fraction near the wall, similar to the RANS-based predictions. This over-prediction highlights the model's detailed resolution of bubble nucleation, growth, and detachment processes. A larger predicted bubble departure diameter therefore results in longer residence times before detachment, leading to a higher evaporative heat flux at the wall. Conversely, a smaller bubble departure diameter reduces the evaporative heat flux, causing an increase in wall temperature to maintain a constant flux. The resulting rise in wall temperature enhances nucleation site density, subsequently increasing the void fraction. In contrast, the MIT model also predicts a wall-peaked profile but shows a lower void fraction near the wall compared to the experimental data, particularly at higher pressures. This discrepancy can be attributed to the model's assumption of extended bubble attachment times, which increase the duration of bubble growth and reduce the frequency of bubble detachment. As a result, fewer bubbles are released into the flow, leading to a lower overall void fraction near the wall. For the Bartolomei and Chanturiya (1967) experiment, all the models show a reasonable agreement with the data in Fig. 5(a), although the force balance model is generally superior. The MIT model indicates later onset boiling, occurring after the pipe's midpoint. This delayed transition to boiling corresponds to the higher predicted wall temperatures Fig. 5(b), which result from a decreasing local evaporation heat flux at the wall. As more heat is absorbed by the liquid phase prior to bubble lift-off, wall temperatures rise accordingly.

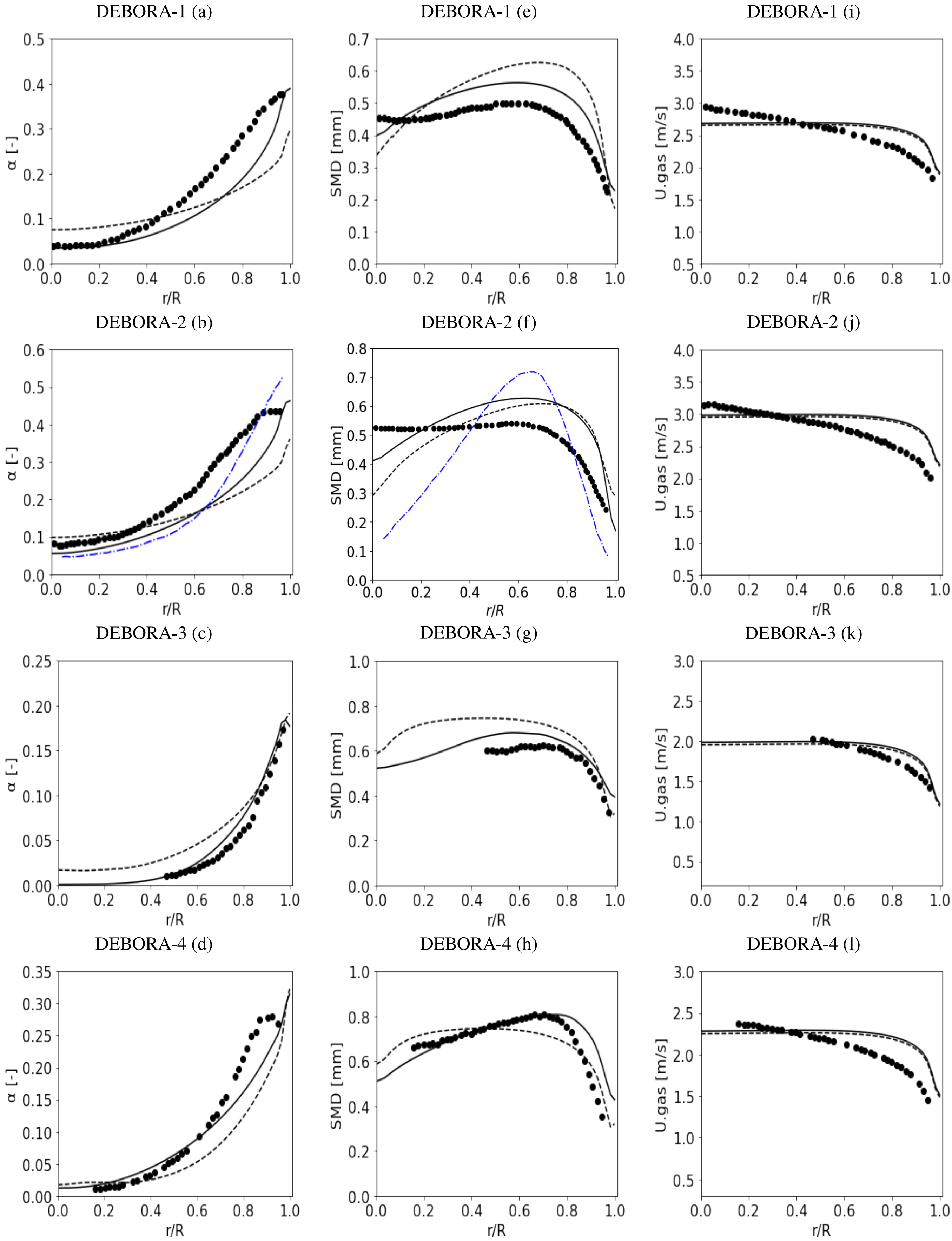

Fig. 4: Radial predictions of (a–d) void fraction, (e–h) Sauter mean diameter, and (i–l) averaged gas velocity for the DEBORA Garnier et al. (2001) experiments: data; – FB; — MIT; – – RANS.

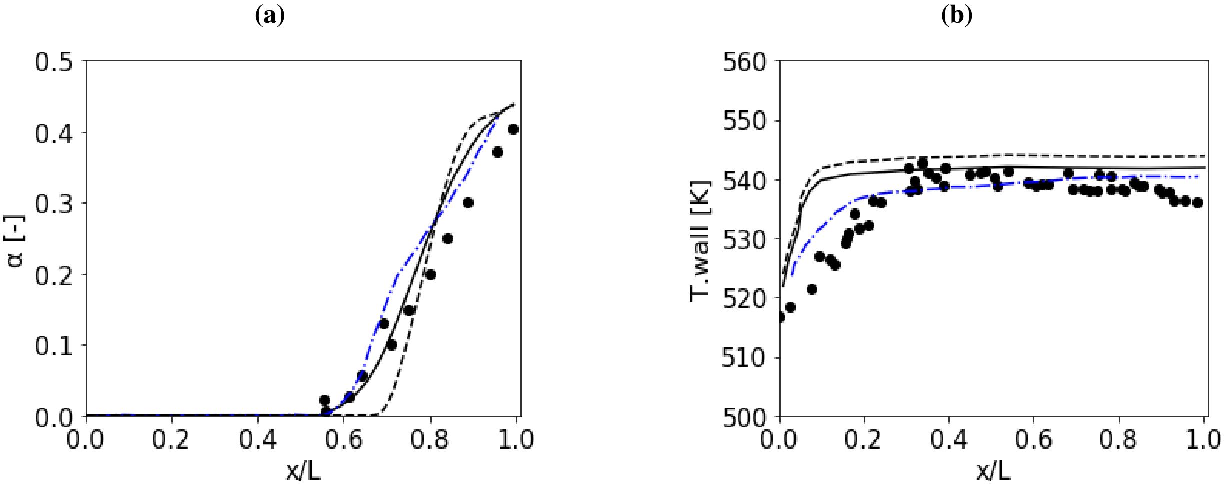

Fig. 5: (a) Averaged void fraction along the pipe, and (b) wall temperature predictions along the heated wall for Bartolomei and Chanturiya (1967) experiment: data; – FB; — MIT; – – RANS.

5.2 Mean Bubble Diameter

The radial distribution of the Sauter mean bubble diameter for the DEBORA Garnier et al. (2001) experiments, shown in Fig. 4(e–h), indicates that bubble size generally increases with distance from the wall, reaches a peak at mid-pipe radius due to bubble coalescence, and then decreases toward the pipe centre where condensation dominates in the colder liquid core of the flow. The force balance model provides superior predictions of this overall trend but slightly under-predicts the bubble diameter near the pipe centre. Both boiling model approaches use the same population balance, and the MIT model exhibits similar trends to the force balance approach, but sometimes over- and under-predicts the peak bubble size compared to the latter model, with similar trends close to the wall. These discrepancies are likely due to limitations in the model's treatment of bubble coalescence and interactions within the bulk flow, which would affect the predicted bubble size, especially in the core region. It also reflects the different void fraction profiles between the two models which affect coalescence and break-up differently. Nonetheless, both models give predictions closer to experimental measurements at lower pressures, underscoring their reliability for less severe operating conditions. In contrast, the RANS-based model significantly under-predict the bubble size across the bulk of the radial profile, with the exception of the peak at $r/R \approx 0.65$. This under-prediction highlights the need for further development of the population balance model used in Colombo et al. (2019), which is coupled with the boiling model, to improve the accuracy of bubble size predictions. Notably, the average bubble diameter near the wall differs significantly between the various models, which reflects the initial bubble departure diameter when the bubbles first detach from the wall and move into the bulk of the flow. This variation in departure diameter can negatively affect the prediction of radial void fraction.

5.3 Mean Gas Velocity

The radial distribution of the mean gas velocity, as shown in Fig. 4(i–l) for the DEBORA Garnier et al. (2001) experiments, shows generally good agreement with the measurements for both models, although there is a slight over-prediction of velocity near the wall. This increase in predictions above experimental values can be attributed to modelling assumptions made for the free-slip boundary condition for bubbles at the wall. In all cases, the maximum bubble velocity occurs at some distance away from the heated wall, with small bubbles arising from nucleation sites on the heated wall having a much lower axial velocity compared to larger bubbles, which result from coalescence processes. The velocity profile remains relatively flat near the pipe centre. This behaviour is consistent with the observation that the Sauter mean diameter in this region is nearly uniform, although experimental profiles do tend to increase slightly as the pipe centre is approached.

5.4 Wall and Liquid Temperatures

The wall temperature predictions along the heated wall for the DEBORA Garnier et al. (2001) experiments are shown in Fig. 6(a-d). Both the force balance and MIT models tend to over-predict the wall temperature, with the RANS-based approach showing the highest over-predictions. However, all models capture the gradual rise in wall temperature along the heated pipe length. The force model predicts higher wall temperatures compared to the MIT model. This is likely due to its higher predicted nucleation site density and bubble departure frequency, which increase the evaporative heat flux at the wall Eq. 30. Since the predicted bubble departure diameters are relatively close between the two models, the difference in wall temperature is mainly controlled by the activity of nucleation sites and detachment rates. However, the trend reverses for the Bartolomei and Chanturiya (1967) experiment results shown in Fig. 5(b) where the MIT model predicts higher wall temperatures than those of the force balance model. Experimental temperatures exhibit a rapid increase in the early regions of the pipe, followed by a levelling off and a slight decline towards the pipe outlet. Both the mechanistic and MIT models roughly follow the experimental trend, capturing the rise in wall temperature close to the pipe inlet, although the rate of increase is significantly over-estimated. This increase is primarily influenced by local flow acceleration and changes in heat transfer mechanisms.

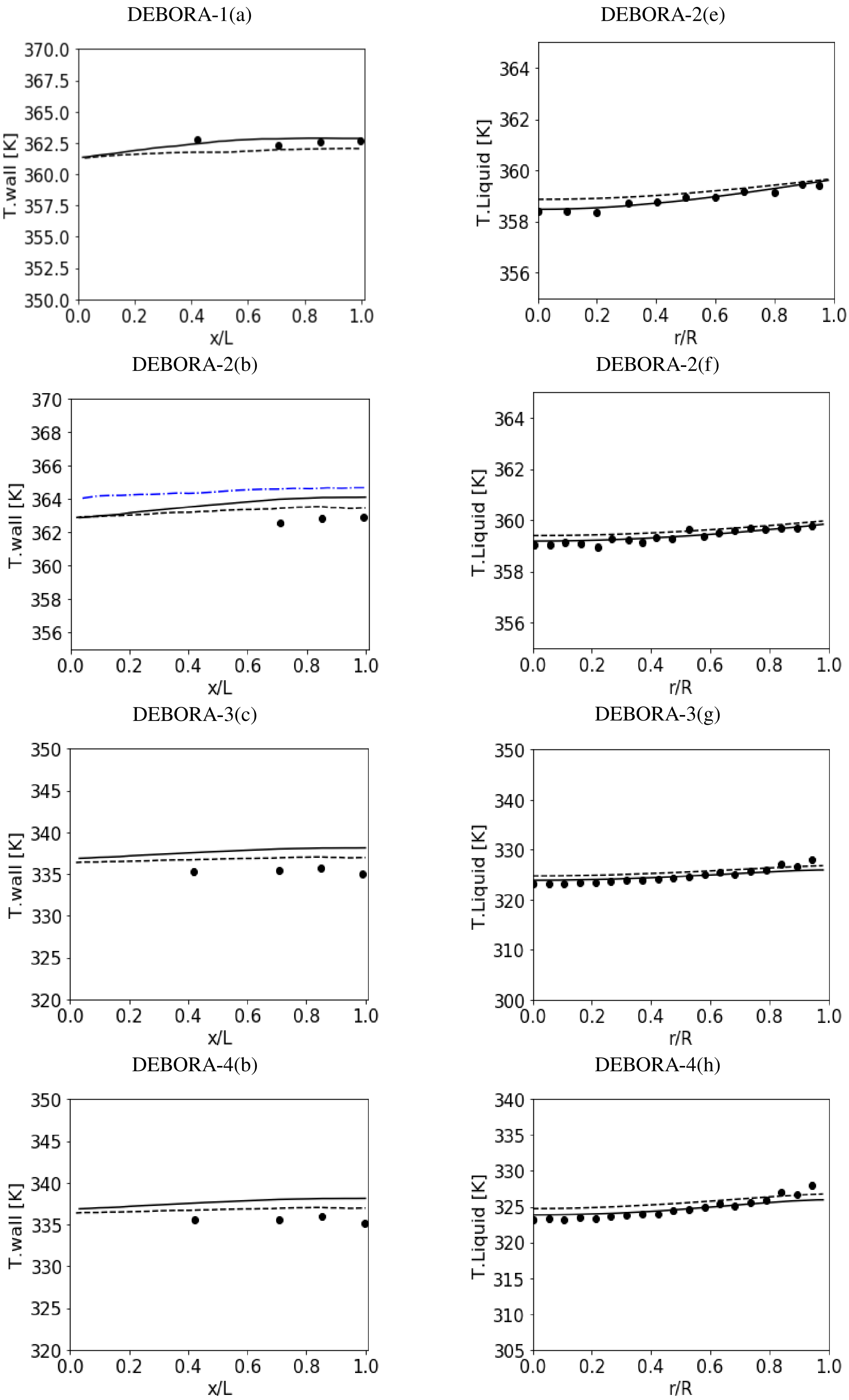

Fig. 6: (a-d) Temperature predictions along the heated wall, and (e-h) radial predictions of liquid temperature for the DEBORA Garnier et al. (2001) experiments: data; – FB; — MIT; – – RANS.

The radial distributions of liquid temperature, shown in Fig. 5(e-h) for the DEBORA Garnier et al. (2001) experiments, indicate a thermal gradient near the heated wall that gradually decreases toward the pipe centre. Both the force balance and MIT models are in good agreement with the measurements. Additionally, across the whole radial profile, the liquid temperatures predicted by both models are in close agreement, with the force balance model predicting slightly lower temperatures. This small difference is consistent with its higher predicted wall-peaked void fraction. The elevated void fraction in the near-wall region therefore reduces liquid contact with the heated surface, limiting heat transfer to the liquid.

6 Conclusions

This study assessed the predictive capabilities of two boiling models, a mechanistic force balance approach and a reduced correlation-based MIT model, coupled with large eddy simulation for predicting turbulent subcooled flow boiling. Validation against the experiments of Garnier et al. (2001) and of Bartolomei and Chanturiya (1967) demonstrated that both models captured the key trends of void fraction, bubble dynamics, wall and liquid temperature distributions. The mechanistic model showed the highest accuracy in predicting bubble dynamics due to its detailed treatment of heat transfer mechanisms. However, it required greater computational resources compared to the MIT model, which offered a more efficient but less precise alternative. Although the RANS-based approach relies on an averaging methodology and does not fully resolve turbulence and phase interactions, it provides good predictions of certain parameters. However, RANS-based approaches tend to oversimplify the complex, unsteady nature of boiling flows, which reduces their accuracy in predicting key parameters. In contrast, LES offers a more physically realistic representation of turbulent flows by resolving large, energy-containing turbulent structures while modelling only the smaller subgrid-scale eddies. This enhanced turbulence resolution improves the accuracy of predictions for bubble departure dynamics, void fraction distribution, and heat transfer mechanisms, particularly in regions dominated by strong phase interactions and subcooling effects. However, the LES-based approach also exhibits some inaccuracies, especially in terms of wall temperature, indicating the need for further refinement to enhance its predictive accuracy. The study also indicates that enhancements in the population balance model could improve predictions of bubble coalescence, breakup, and size distribution, particularly near the pipe centre where condensation and bubble interactions are significant. Similarly, refining nucleation site density correlations could improve predictions of wall temperature. Incorporating these improvements within an LES framework would further strengthen the model's predictive accuracy. Despite these shortcomings, this work confirms that mechanistic models combined with LES offer a high-fidelity tool for analysing subcooled boiling flows, while reduced correlation models provide a practical balance between accuracy and computational efficiency. These findings support the continued development of predictive boiling models for nuclear and industrial thermal hydraulic applications.

Acknowledgements

This work is supported by the Ministry of Higher Education and Scientific Research of Libya.

References

T. R. Auton. The lift force on a spherical body in a rotational flow. *Journal of Fluid Mechanics*, 183:199–218, 1987. doi: 10.1017/S002211208700260X.

G. G. Bartolomei and V. M. Chanturiya. Experimental study of true void fraction when boiling subcooled water in vertical tubes. *Thermal Engineering*, 14:123–128, 1967.

R. Cole. A photographic study of pool boiling in the region of the critical heat flux. *AIChE Journal*, 6:533–538, 1960. doi: 10.1002/aic.690060405.

M. Colombo and M. Fairweather. Multiphase turbulence in bubbly flows: Rans simulations. *International Journal of Multiphase Flow*, 77:222–243, 2015a. doi: 10.1016/j.ijmultiphaseflow.2015.03.001.

M. Colombo and M. Fairweather. Prediction of bubble departure in forced convection boiling: A mechanistic model. *International Journal of Heat and Mass Transfer*, 85:135–146, 2015b. doi: 10.1016/j.ijheatmasstransfer.2015.01.103.

M. Colombo and M. Fairweather. Accuracy of eulerian-eulerian, two-fluid cfd boiling models of subcooled boiling flows. *International Journal of Heat and Mass Transfer*, 103:28–44, 2016. doi: 10.1016/j.ijheatmasstransfer.2016.06.098.

M. Colombo, R. Thakrar, M. Fairweather, and S. P. Walker. Assessment of semi-mechanistic bubble departure diameter modelling for the cfd simulation of boiling flows. *Nuclear Engineering and Design*, 344:15–27, 2019. doi: 10.1016/j.nucengdes.2019.01.014.

M. G. Cooper and A. J. P. Lloyd. The microlayer in nucleate pool boiling. *International Journal of Heat and Mass Transfer*, 12: 895–913, 1969. doi: 10.1016/0017-9310(69)90154-9.

M. A. L. de Bertodano. Two fluid model for two-phase turbulent jets. *Nuclear Engineering and Design*, 179:65–74, 1998.

V. K. Dhir. Boiling heat transfer. *Annual Review of Fluid Mechanics*, 30:365–401, 1998. doi: 10.1146/annurev.fluid.30.1.365.

X. Fang, Y. Yuan, A. Xu, L. Tian, and Q. Wu. Review of correlations for subcooled flow boiling heat transfer and assessment of their applicability to water. *Fusion Engineering and Design*, 122:52–63, 2017. doi: 10.1016/j.fusengdes.2017.09.008.

J. Garnier, E. Manon, and G. Cubizolles. Local measurements on flow boiling of refrigerant 12 in a vertical tube. *Multiphase Science and Technology*, 13:1–111, 2001. doi: 10.1615/MultScienTechn.v13.i1-2.10.

M. Germano, U. Piomelli, P. Moin, and W. H. Cabot. A dynamic subgrid-scale eddy viscosity model. *Physics of Fluids A: Fluid Dynamics*, 3:1760–1765, 1991. doi: 10.1063/1.857955.

C. J. Greenshields. *OpenFOAM User Guide*. OpenFOAM Foundation, 2019. URL https://doc.cfd.direct/openfoam/user-guide-v7.

T. Hibiki and M. Ishii. Active nucleation site density in boiling systems. *International Journal of Heat and Mass Transfer*, 46: 2587–2601, 2003. doi: 10.1016/S0017-9310(03)00031-0.

H. A. Jakobsen, S. Grevskott, and H. F. Svendsen. Modeling of vertical bubble-driven flows. *Industrial & Engineering Chemistry Research*, 36:4052–4074, 1997. doi: 10.1021/ie970276o.

A. Kader. Temperature and concentration profiles in fully turbulent boundary layers. *International Journal of Heat and Mass Transfer*, 24:1541–1544, 1981. doi: 10.1016/0017-9310(81)90220-9.

J. F. Klausner, R. Mei, D. M. Bernhard, and L. Z. Zeng. Vapor bubble departure in forced convection boiling. *International Journal of Heat and Mass Transfer*, 36:651–662, 1993. doi: 10.1016/0017-9310(93)80041-R.

R. Kommajosyula. *Development and assessment of a physics-based model for subcooled flow boiling with application to CFD*. PhD thesis, Massachusetts Institute of Technology, 2020.

E. Krepper, D. Lucas, D. Frank, HM. Prasser, and P.J. Zwart. The inhomogeneous musig model for the simulation of polydispersed flows. *Nuclear Engineering and Design*, 238:1690–1702, 2008. doi: 10.1016/j.nucengdes.2008.01.004.

N. Kurul and M. Z. Podowski. Multidimensional effects in forced convection subcooled boiling. In *Proceedings of the Ninth International Heat Transfer Conference*, pages 21–26, 1990. doi: 10.1615/IHTC9.40.

F. Lehr, M. Millies, and D. Mewes. Bubble-size distributions and flow fields in bubble columns. *AIChE Journal*, 48:2426–2443, 2002. doi: 10.1002/aic.690481103.

M. Lemmert and J. M. Chawla. Influence of flow velocity on surface boiling heat transfer coefficient. In E. Hahne and U. Grigull, editors, *Heat Transfer in Boiling*, pages 237–247. Hemisphere, Washington, D.C., 1977.

A. Leonar. Energy cascade in large-eddy simulations of turbulent fluid flows. in f. n. frenkiel and r. e. munn, editors. *Advances in Geophysics, Turbulent Diffusion in Environmental Pollution*, pages 237–248, 1975. doi: 10.1016/S0065-2687(08)60464-1.

R. Mei and J. F. Klausner. Unsteady force on a spherical bubble at finite reynolds number with small fluctuations in the free-stream velocity. *Physics of Fluids A: Fluid Dynamics*, 4:63–70, 1992. doi: 10.1063/1.858501.

J. Owoeye and D. Schubring. Cfd analysis of bubble microlayer and growth in subcooled flow boiling. *Nuclear Engineering and Design*, 304:151–165, 2016. doi: 10.1016/j.nucengdes.2016.04.027.

M. Pham, G. Bois, F. Francois, and E. Baglietto. Assessment of state-of-the-art multiphase cfd modeling for subcooled flow boiling in reactor applications. *Nuclear Engineering and Design*, 411:112379, 2023. doi: 10.1016/j.nucengdes.2023.112379.

M. S. Plesset and S. A. Zwick. The growth of vapor bubbles in superheated liquids. *Journal of Applied Physics*, 25:493–500, 1954. doi: 10.1063/1.1721668.

M. J. Prince and H. W. Blanch. Bubble coalescence and break-up in air-sparged bubble columns. *AIChE Journal*, 36:1485–1499, 1990. doi: 10.1002/aic.690361004.

A. Prosperetti and G. Tryggvason. *Computational Methods for Multiphase Flow*. Cambridge University Press, 2009.

W. E. Ranz and W. R. Marshall. The evaporation from drops. part ii. *Chemical Engineering Progress*, 48:173–180, 1952.

Y. Sato, M. Sadatomi, and K. Sekoguchi. Momentum and heat transfer in two-phase bubble flow - i. theory. *International Journal of Multiphase Flow*, 7:167–177, 1981. doi: 10.1016/0301-9322(81)90003-3.

D. B. Spalding. A single formula for the law of the wall. *Journal of Applied Mechanics*, 28:455–458, 1961.

R. Sugrue and J. Buongiorno. A modified force-balance model for prediction of bubble departure diameter in subcooled flow boiling. *Nuclear Engineering and Design*, 305:717–722, 2016. doi: 10.1016/j.nucengdes.2016.04.017.

V. I. Tolubinsky and D. M. Kostanchuk. Vapour bubbles growth rate and heat transfer intensity at subcooled water boiling. In *Proceedings of the 4th International Heat Transfer Conference*, pages 1–11, New York, 1970. Begell House. doi: 10.1615/IHTC4.250.

A. Tomiyama, I. Kataoka, I. Zun, and T. Sakaguchi. Drag coefficients of single bubbles under normal and micro gravity conditions. *JSME International Journal Series B*, 41:472–479, 1998.

G. H. Yeoh, S. Vahaji, S. C. P. Cheung, and J. Y. Tu. Modeling subcooled flow boiling in vertical channels at low pressures – part 2: Evaluation of mechanistic approach. *International Journal of Heat and Mass Transfer*, 75:754–768, 2014. doi: 10.1016/j.ijheatmasstransfer.2014.03.017.

B. J. Yun, A. Splawski, S. Lo, and C.-H. Prediction of a subcooled boiling flow with advanced two-phase flow models. *Nuclear Engineering and Design*, 253:351–359, 2012. doi: 10.1016/0017-9310(81)90220-9.

K. Zhou, C. Coyle, J. Li, J. Buongiorno, and W. Li. Flow boiling in vertical narrow microchannels of different surface wettability characteristics. *International Journal of Heat and Mass Transfer*, 109:103–114, 2017. doi: 10.1016/j.ijheatmasstransfer.2017.01.111.